

1 **FRONT MATTER**

2

3 **Title**

4 Boiling histotripsy induces dendritic cell activation and acquisition of antigen in tumor draining
5 lymph nodes

6

7 **Authors**

8 Eric A. Thim^{1,†}, Lydia E. Petricca^{2,†}, Fátima Rivera-Escalera³, Alexander S. Mathew¹, Michael R.
9 Elliott³, Timothy N. J. Bullock^{2,*}, Richard J. Price^{1,*}

10

11 **Affiliations**

12 1. Department of Biomedical Engineering, University of Virginia, Charlottesville, VA 22908.

13 2. Department of Pathology, University of Virginia, Charlottesville, VA 22908.

14 3. Department of Microbiology, Immunology and Cancer Biology, University of Virginia,
15 Charlottesville, VA 22908.

16 †. These authors contributed equally: E. Andrew Thim and Lydia E. Petricca.

17

18 *Corresponding Authors:

19 Richard J. Price, Ph.D.

20 Department of Biomedical Engineering

21 Box 800759, Health System

22 University of Virginia

23 Charlottesville, VA 22908, USA

24 Telephone: (434) 924-0020

25 Email: rprice@virginia.edu

26 ORCID: 0000-0002-0237-2102

27

28 Timothy N. J. Bullock, Ph.D.

29 Department of Pathology

30 Box 801386, Health System

31 University of Virginia

32 Charlottesville, VA 22908, USA

33 Telephone: (434) 982-1932

34 Email: tb5v@virginia.edu

35 ORCID: 0000-0001-6141-3261

36

37

38

39

40

41

42

43

44

45

46

Abstract

47 Boiling histotripsy (BH), a mechanical focused ultrasound ablation strategy, can elicit
48 intriguing signatures of anti-tumor immunity. However, the influence of BH on dendritic cell
49 function is unknown, compromising our ability to optimally combine BH with immunotherapies to
50 control metastatic disease. Here, by applying BH to B16F10 melanoma expressing a ZsGreen
51 antigen in a monotherapy protocol that elicits abscopal tumor control, we observed a marked
52 increase in antigen acquisition by multiple phagocytic immune cells, including conventional
53 dendritic cells (i.e. cDC1s and cDC2s), in tumor draining lymph nodes. Further, BH activated
54 (CD86 expression) cDC1s and cDC2s in a tumor antigen-dependent fashion and liberated an
55 antigen complex that likely contains a DAMP(s). In all, these results shed considerable light on
56 how BH influences the cancer immunity cycle and offer new insight into how to best combine BH
57 with immunotherapies.

58

59

60 **Teaser**

61 Boiling histotripsy monotherapy yields abscopal melanoma control and markedly augments anti-
62 tumor dendritic cell maturation.

63

64

65 Introduction

66 Melanoma diagnoses continue to rise, with ~105,000 new cases predicted for 2023. Despite
67 significant recent advances in treatment with targeted therapies and immunotherapies, melanoma
68 patients who experience distant metastatic spread still have only a 32% 5-year survival rate (1).
69 Immunotherapies aimed at increasing the endogenous immune response against melanoma are now
70 standard in the clinical armamentarium. Such immunotherapies have a variety of targets, including
71 programmed death receptor/ligand-1 (PD-1/PD-L1), cytotoxic T-lymphocyte associated protein 4
72 (CTLA-4), and interleukin 2 (IL-2) (2, 3). However, many patients still do not experience the
73 survival benefits these therapies can offer. Their tumors, which are collectively termed
74 immunologically “cold” (2, 4), typically have a paucity of T lymphocyte (T cell) infiltration.
75 Limited T cell presence within tumors can be the result of inadequate tumor antigen acquisition and
76 presentation by dendritic cells (DC), which serve as obligate activators of tumor-specific T cells; a
77 failure of DC to traffic to lymph nodes to interact with the T cell repertoire; a surplus of
78 immunosuppressive cells (e.g. regulator T cells [Tregs] and myeloid derived suppressor cells
79 [MDSCs]) that suppress T and DC activity; and/or an inability of activated T cells to traffic to and
80 persist in tumors (2, 4). There is a clear need for a treatment modality that can transform a “cold
81 tumor” into a “hot tumor” for increased responses to immunotherapies.

82 Focused ultrasound (FUS), a term referred to here as the concentration of acoustic energy
83 into a small focus to create bioeffects in tumor tissue, holds considerable promise as a minimally-
84 invasive means for transforming “cold” tumors into “hot” tumors, while limiting off-target and side
85 effects. FUS is a highly versatile treatment modality. By tuning FUS application parameters, one
86 can generate primarily thermal (e.g., hyperthermia and coagulative necrosis) or mechanical (e.g.,
87 sonoporation and microvascular ablation) bioeffects in tumor tissue. Further, FUS is not limited by
88 dose and may be repeated often due to its non-ionizing nature (5–7).

89 Boiling histotripsy (BH) is a mechanical tissue fractionization FUS regimen that acts
90 through high-pressure, millisecond long FUS pulses. BH produces a millimeter-sized vapor bubble
91 that initiates pre-focal inertial cavitation, which is then theorized to be the predominant source of
92 tissue fractionation and homogenization (8, 9, 18, 10–17). Because BH produces cavitating bubbles
93 from endogenous gases and fluids, the need to deliver exogenous microbubble contrast agents, as
94 in microbubble cavitation FUS regimens, is obviated. Since BH does not cause thermal
95 accumulation and occurs on a short timescale, it can create sharp treatment margins and minimize
96 peripheral tissue damage. For instance, BH has a transition zone on the order of a few cell lengths
97 (16).

98 BH has also been reported to exert beneficial immune responses. For example, BH increases
99 DC infiltration into tumors one- and two-days post-treatment (10). BH also likely promotes
100 conditions that support DC migration, as demonstrated by the increased presence of intratumorally-
101 injected DC in the tumor draining lymph node (TDLN) of MC-38 colorectal tumor-bearing
102 mice (10). BH also increases T cell activity as splenocytes from BH-treated mice exhibit increased
103 anti-tumor cytotoxicity compared to sham and thermal ablation (TA) treated mice (10), suggesting
104 that BH induces a higher degree of immunogenicity. MC-38 tumor cells targeted with BH in vitro
105 release danger associated molecular patterns (DAMPs), like ATP and HSP60, stimulating
106 cocultured DCs to upregulate CD80 and CD86 costimulatory molecules and increase IL-12
107 production (8). Moreover, CD86 and PD-L1 expression on DCs increased 48 hr post-BH treatment
108 in TDLNs of mice with EG.7-OVA lymphoma. When a toll-like receptor (TLR) agonist (cytidyl
109 guanosyl [CpG]) was combined with BH, CD80, CD86, and PD-L1 expression increased compared
110 to sham and compared to CpG⁻ controls (19). In murine renal cell carcinoma, BH increases CD8⁺
111 T-cell infiltration (9). BH has also been reported to outperform TA in controlling breast tumor
112 growth (20). These immunological findings, combined with the versatile and minimally-invasive
113 nature of BH, showcase BH as an attractive FUS modality for augmenting immunotherapy.

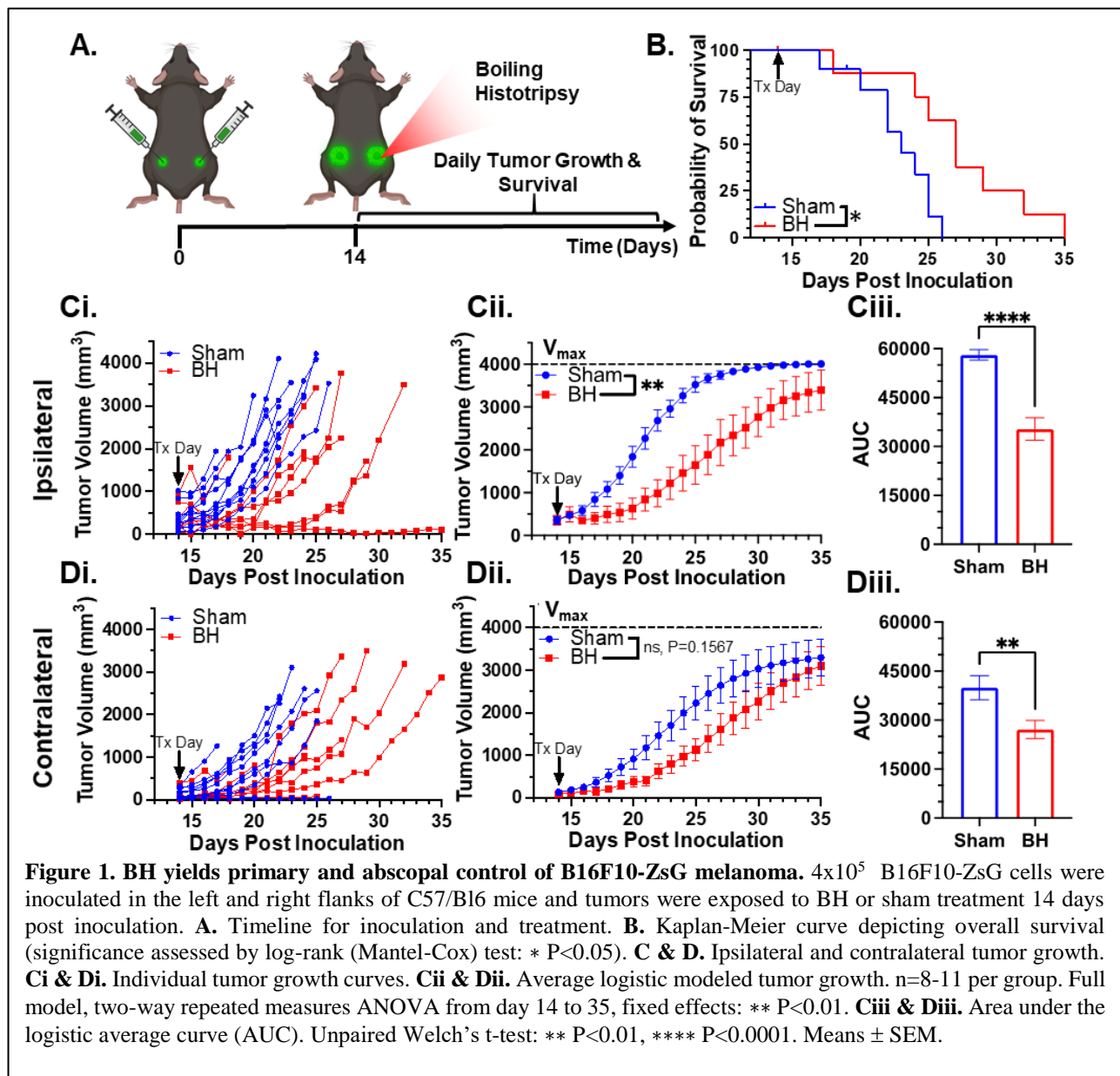
114 However, despite the clear potential for BH to stimulate adaptive immune responses against
115 solid tumors, there are still important gaps in our understanding of how BH affects key elements of
116 the cancer-immunity cycle. Until these knowledge gaps are filled, our ability to optimally combine
117 immunotherapies with BH to drive systemic anti-tumor immune responses will be compromised.
118 In particular, many of these gaps center on how and where BH affects tumor antigen trafficking
119 and acquisition. For example, we do not yet understand the time course of BH-driven tumor antigen
120 trafficking to TDLNs and subsequent acquisition by antigen presenting cells (APCs). Acquiring
121 such knowledge will be invaluable for defining the time course of administration of
122 immunotherapies intended to synergize with BH via augmented tumor antigen acquisition by APCs,
123 as well as for designing studies aimed at defining how BH modulates phagocytic activity of APCs.
124 Furthermore, it is unclear as to whether/how such BH-liberated tumor antigen is partitioned
125 amongst DC subsets (i.e., cDC1 vs. cDC2). Because CD8⁺ T cells are generally thought to be
126 primarily activated by cDC1s (21–23), while CD4⁺ T cells require cDC2s for initial priming (21),
127 defining both the activation and relative acquisition of tumor antigen by each DC subset may help
128 identify opportunities for therapeutically tuning the relative contributions of effector and helper T
129 cells to the BH-induced anti-tumor immunity. Finally, it is also unknown as to whether DC
130 maturation is affected by the acquisition of BH-liberated tumor antigen in vivo and whether tumor
131 antigen is preferentially acquired by DCs in the tumor microenvironment or in the TDLN. Such
132 knowledge will inform proper tuning of the intensity and volumetric fraction of BH to optimally
133 elicit anti-tumor immunity. For example, if DC activation depends on tumor antigen acquisition, a
134 more aggressive liberation of antigen by BH would be warranted. On the other hand, evidence for
135 DC acquisition of antigen in the tumor microenvironment could suggest that reducing the
136 volumetric fraction of BH treatment could improve anti-tumor immunity by sparing intratumoral
137 DCs from ablation.

138 Here, we directly address these key gaps in our understanding of how BH drives anti-tumor
139 immunity in a mouse model of melanoma. By employing a B16F10 cell line that stably expresses
140 ZsGreen (ZsG) (i.e., B16F10-ZsG) as a model tumor antigen in combination with a sparse scan BH
141 treatment scheme that elicits abscopal tumor control, we specifically investigated (i) tumor BH-
142 induced antigen drainage to lymph nodes, (ii) tumor antigen acquisition and partitioning by
143 phagocytic immune cells and DC subsets in the TDLN, (iii) DC activation as a function of tumor
144 antigen acquisition, and (iv) the trafficking potential of antigen positive DCs through CD8 α ⁺ (tissue
145 resident) and CD103⁺ (migratory) cDC1 subpopulations. Our findings yield new insights into DC
146 behavior in the setting of abscopal tumor control, while also providing guidance for how
147 immunotherapeutic manipulations may be rationally combined with BH to further control of
148 systemic disease.

149 Results

151 Boiling Histotripsy Elicits Primary and Abscopal Tumor Control

152 We first developed a BH treatment protocol that yields abscopal control of distal disease for
153 a melanoma model (B16F10-ZsG) expressing a fluorescent protein (ZsG) that could be leveraged
154 to assess tumor antigen trafficking/acquisition by APCs. Because the B16F10-ZsG melanoma
155 model was deployed for all experiments in this study, it is henceforth often referred to as “tumor”
156 or “melanoma.” “Primary” refers to ipsilateral (treated) while “secondary” refers to contralateral
157 (untreated). The primary tumors were chosen for treatment as the larger of the two tumors. When
158 applied to the ipsilateral tumor in a bilateral setting at 14 days post-inoculation, our BH regimen
159 (Figure 1A; FUS parameters provided in Figure S1) significantly improved survival (Figure 1B)
160 and controlled ipsilateral tumors (Figure 1Ci-ii), with the “area under the curve” (AUC) metric
161 showing a highly significant ~40% reduction in integrated tumor burden (Figure 1Ciii). For
162 contralateral tumors not directly exposed to BH, multi-variate statistical analysis of the modeled



163 growth curves showed a strong trend toward growth control (Figure 1Di-ii), with the AUC metric
 164 (Figure 1Diii) yielding a significant reduction in integrated contralateral tumor burden. In all, this
 165 indicates that our BH monotherapy protocol elicits abscopal tumor control in this model.

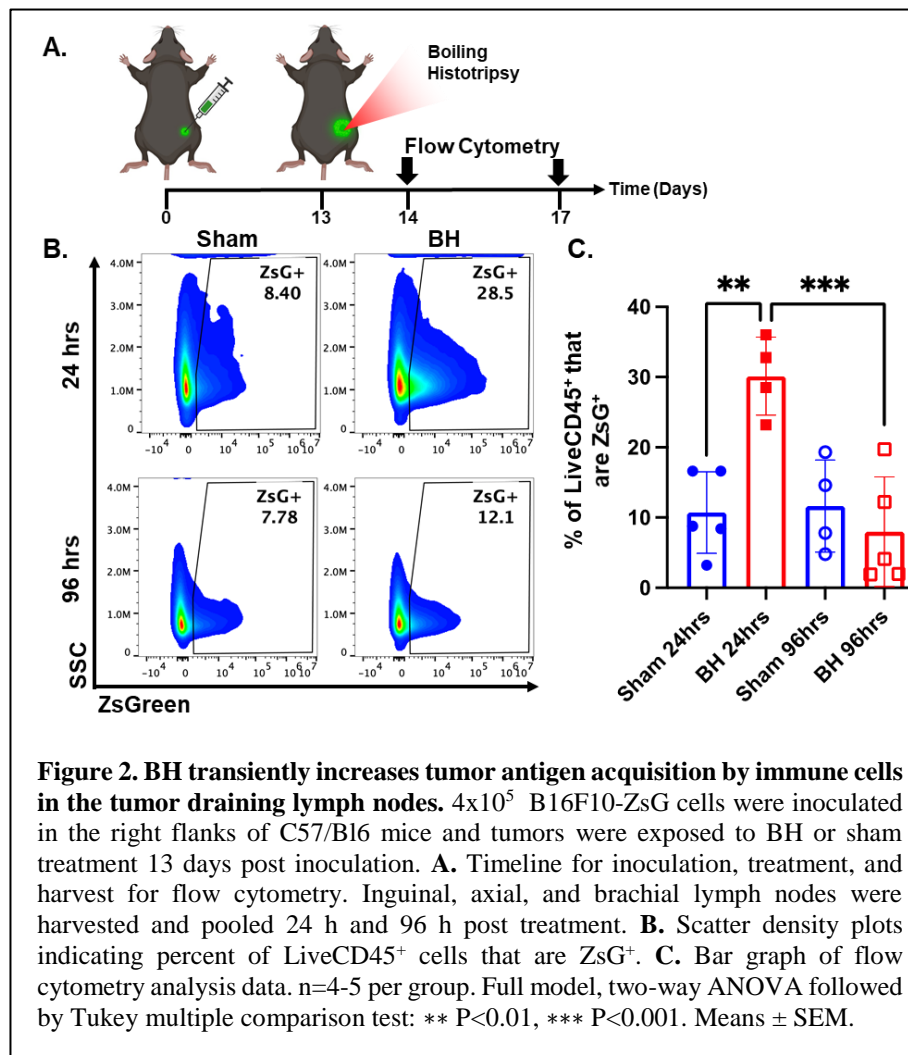
167 Boiling Histotripsy Transiently Increases Tumor Antigen Acquisition by Immune Cells

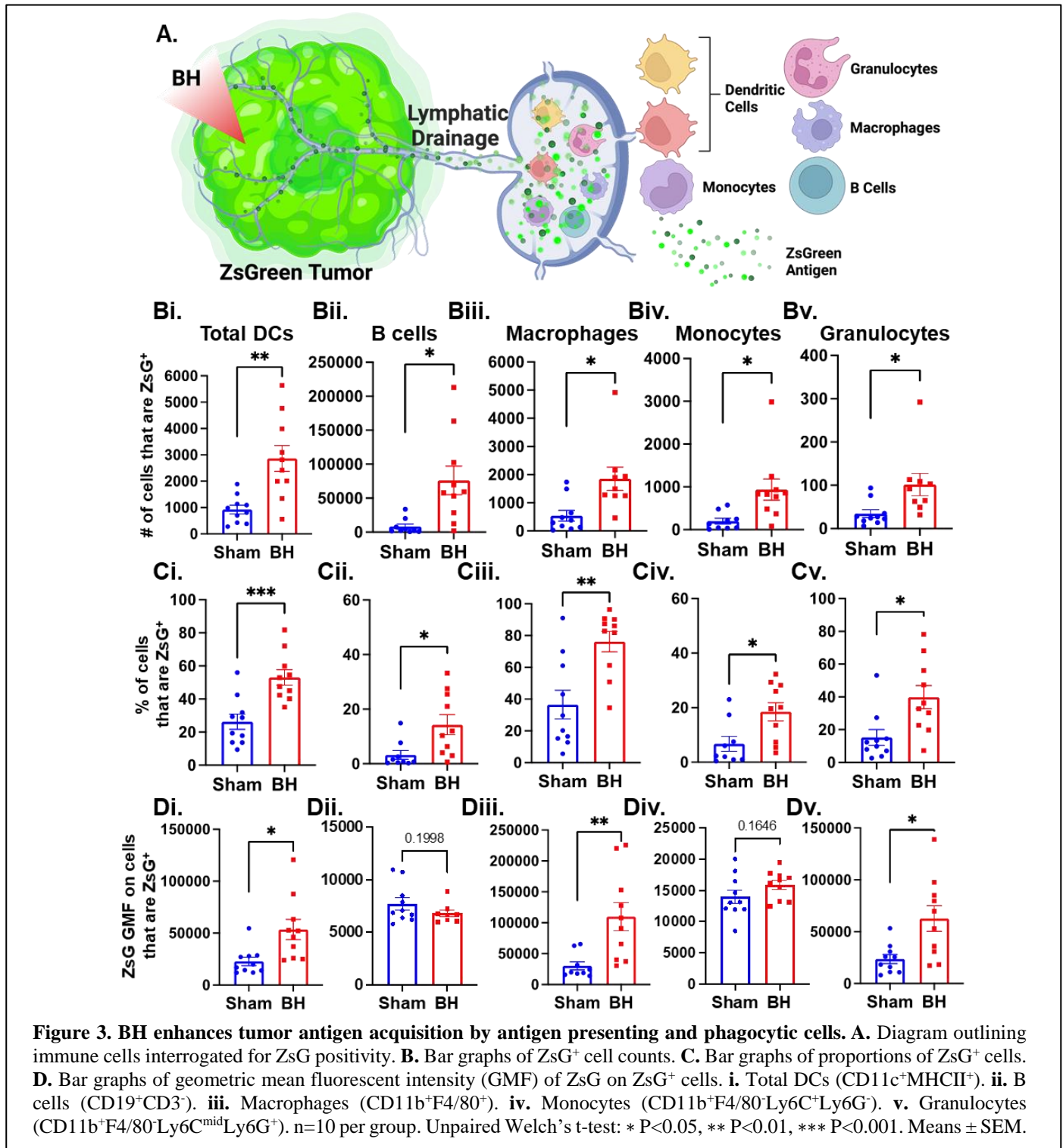
168 After establishing that this BH treatment regimen controls distal tumor growth (Figure 1),
 169 we examined the time course of antigen acquisition by immune cells ($CD45^+$) in the TDLNs in a
 170 unilateral B16F10-ZsG model in response to BH (Figure 2A). The ZsG fluorescent antigen allowed
 171 for the tracking of antigen in TDLN cells (Figure 2B; gating strategy provided in Figure S2). We
 172 found that BH elicited a nearly three-fold increase in the proportion of $ZsG^+ CD45^+$ immune cells
 173 24 h post-treatment (Figure 2C). However, by 96 h, ZsG^+ antigen presence in $CD45^+$ cells returned
 174 to near baseline levels. Interestingly, the contralateral non-TDLN (CLN) exhibited low-levels of
 175 baseline ZsG antigen (Figure S3), with the proportion of $CD45^+$ cells that are ZsG^+ being ~15-fold
 176 lower than those in the baseline ipsilateral TDLN. Nonetheless, BH did not alter contralateral tumor
 177 antigen presence, indicating that BH does not increase circulating tumor antigen. Further, BH did

not increase the number or proportion of CD45⁺ZsG⁺ cells either in the CLN or TDLN (Figure S4), suggesting that BH did not promote dissemination of tumor cells to lymph nodes, mitigating the concern that mechanically destroying tumors could increase the release of tumor cells to distant sites (e.g., TDLNs) (24–26).

Boiling Histotripsy Induces Antigen Acquisition by Multiple Phagocytic Cell Types

We next asked which immune cell types in the TDLN acquired tumor antigen at 24 h after BH, as antigen partitioning after BH is currently unknown and could significantly impact anti-tumor immunity (Figure 3A). We specifically examined ZsG acquisition by antigen presenting and phagocytic cells such as DCs, B cells, macrophages, monocytes, and granulocytes (gating strategy provided in Figure S5.) For all APC and phagocytic cell types examined, we observed an increase in the number (Figure 3Bi-v) and proportion (Figure 3Ci-v) of ZsG⁺ cells 24 h post BH treatment. As a negative control for ZsG acquisition, we examined ZsG positivity of a non-APC and non-phagocytic cell type (CD8⁺ T cells; Figure S6A). As expected, we found an extremely low proportion of CD8⁺ T cells acquired ZsG, and BH did not change this proportion (Figure S6B). For APCs, the number and proportion of ZsG⁺ total DCs increased, by 2.5-fold and 2-fold, respectively; ZsG⁺ B cells increased by 9-fold in number and 3-fold in proportion; ZsG⁺ macrophages increased by 3-fold in number and 2-fold in proportion; ZsG⁺ monocytes increased by 4.5-fold in number and 2.5-fold in proportion; ZsG⁺ granulocytes increased by 3-fold in number and 2.5-fold in proportion. Further, the amount of antigen each cell type acquired, as quantified by geometric mean fluorescent (GMF) intensity, increased in DCs (2-fold), macrophages (3.5-fold) and granulocytes (2.5-fold) as a result of BH treatment. Interestingly, despite B cells exhibiting the greatest increase in both the number and proportion of cells acquiring ZsG, no difference in the GMF of ZsG was observed. This suggests that BH potentiates ZsG⁻ B cells to acquire antigen (i.e., B cells become ZsG⁺) rather than the amount of antigen that each B cell acquires. Altogether, this analysis shows that BH enhanced ZsG tumor antigen presence in all examined phagocytic and antigen presenting cell types in TDLNs 24 h post treatment.





227 Conventional DCs Acquire Antigen in Response to Boiling Histotripsy

228 We observed an almost 3-fold increase in the number and proportion of DCs that acquired
 229 ZsG after BH (Figure 2Bi and 2Ci). DC subsets (i.e., cDC1 and cDC2) have distinct phenotypes
 230 and functions that can differentially affect anti-tumor immune responses (Figure 4A) (cDC1: CD8⁺
 231 T cell activation and CD4⁺ T cell licensing; cDC2: CD4⁺ T cell priming). Thus, to understand
 232 whether DCs differentially acquire BH-liberated tumor antigen, we separated cDC1s (XCR1⁺) and
 233 cDC2s (XCR1⁻CD11b⁺SIRPα⁺) from the total DC population (gating strategy provided in Figure
 234 S7) and measured changes in ZsG expression (Figure 4B) for cDC1s (Figure 4B; Top) and cDC2s

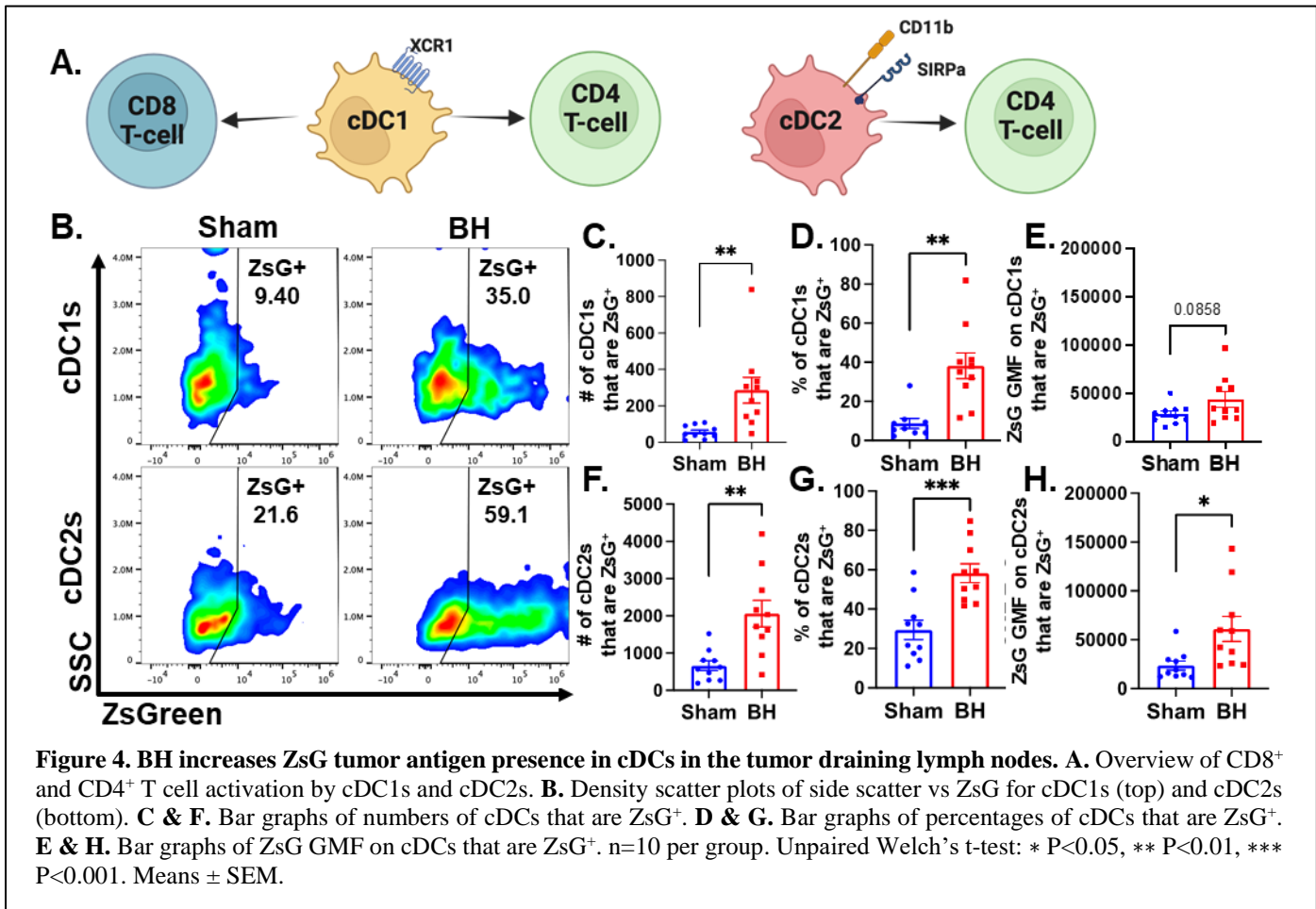
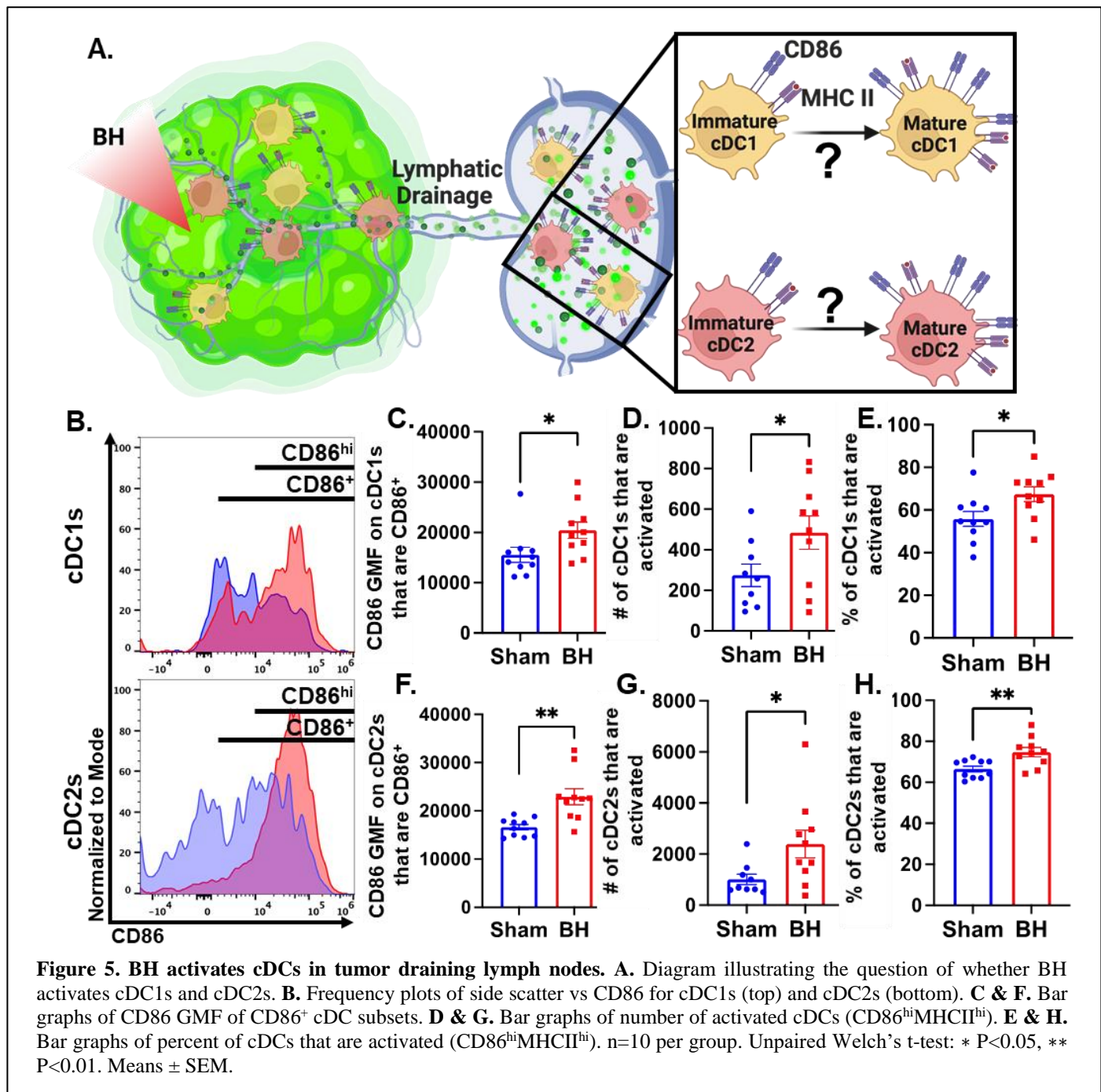


(Figure 4B; Bottom) 24 h post-treatment. When quantified, the number and proportion of both cDC1s (Figure 4C-D) and cDC2s (Figure 4F-G) that are ZsG⁺ increased significantly with BH. When examining GMF, the amount of ZsG per cell on cDC2s significantly increased with BH (Figure 4H), while the amount of ZsG per cell on cDC1s trended toward an increase (Figure 4E). This shows that within the DC compartment, BH enhanced tumor antigen expression by both cDC1s and cDC2s.

Boiling Histotripsy Activates cDCs

Knowing that both cDC1s and cDC2s exhibit enhanced tumor antigen acquisition after BH, we next asked whether BH elicited changes in the activation status of cDCs present within the TDLNs 24 h post treatment. cDC1 and/or cDC2 activation, which has not been previously reported or characterized in response to BH, is an essential step in the cancer immunity cycle as it is required for effective T cell priming and activation to elicit anti-tumor immunity. As CD86 is a co-stimulatory molecule upregulated on the surface of DCs as they undergo activation and maturation (Figure 5A), we first examined CD86 presence on the surface of cDC1s and cDC2s (Figure 5B). We found that BH stimulates greater overall CD86 expression per cell in both cDC subsets (Figure 5C and F). Within the subset of CD86⁺ cDCs, we identified a secondary CD86^{hi} population (Figure 5B and S6). This enabled us to use CD86^{hi}MHCII^{hi} (Figure S7) as the designation for activated and mature DCs. While both cDC1s and cDC2s had a high proportion of activated cells at baseline (~55% [Figure 5E] and ~65% [Figure 5H], respectively), we found that BH elevates CD86 expression per cell in both cDC subsets (Figure 5C and F). Furthermore, we found that BH stimulates an increase in the number of CD86^{hi} cDC1s (Figure 5D) and cDC2s (Figure 5G), as well



257 as a greater proportion of activated cDC1s (Figure 5E) and cDC2s (Figure 5H). Overall, these
 258 results demonstrate that BH enhances the activation of both cDC subsets in TDLN.

260 Conventional Dendritic Cell Activation by Boiling Histotripsy Depends on Tumor Antigen 261 Acquisition

262 Because we observed that BH elicits increased total DC antigen acquisition and cDC
 263 activation, we asked whether BH-induced cDC activation was dependent on ZsG tumor antigen
 264 acquisition (Figure 6A). If not, and ZsG⁻ cDC also exhibit increased activation with BH, it would
 265 suggest that BH treatment liberates immunostimulatory molecules that are available to all cDC. To
 266 address this question, we analyzed CD86 expression on ZsG⁻ cDC subsets (Figure 6B). We
 267 observed no differences in cDC CD86 expression (Figure 6C and F) or changes in the number

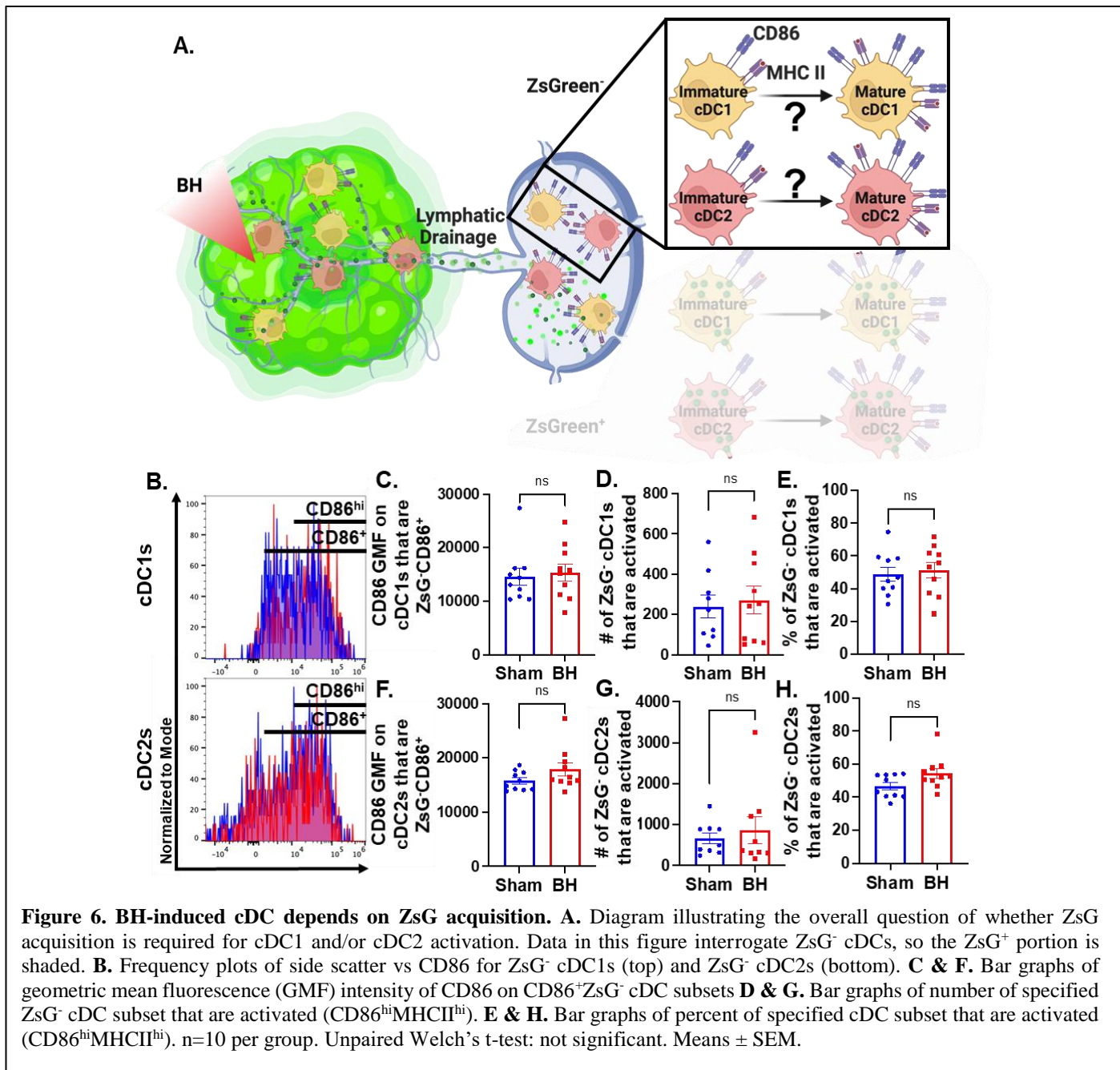
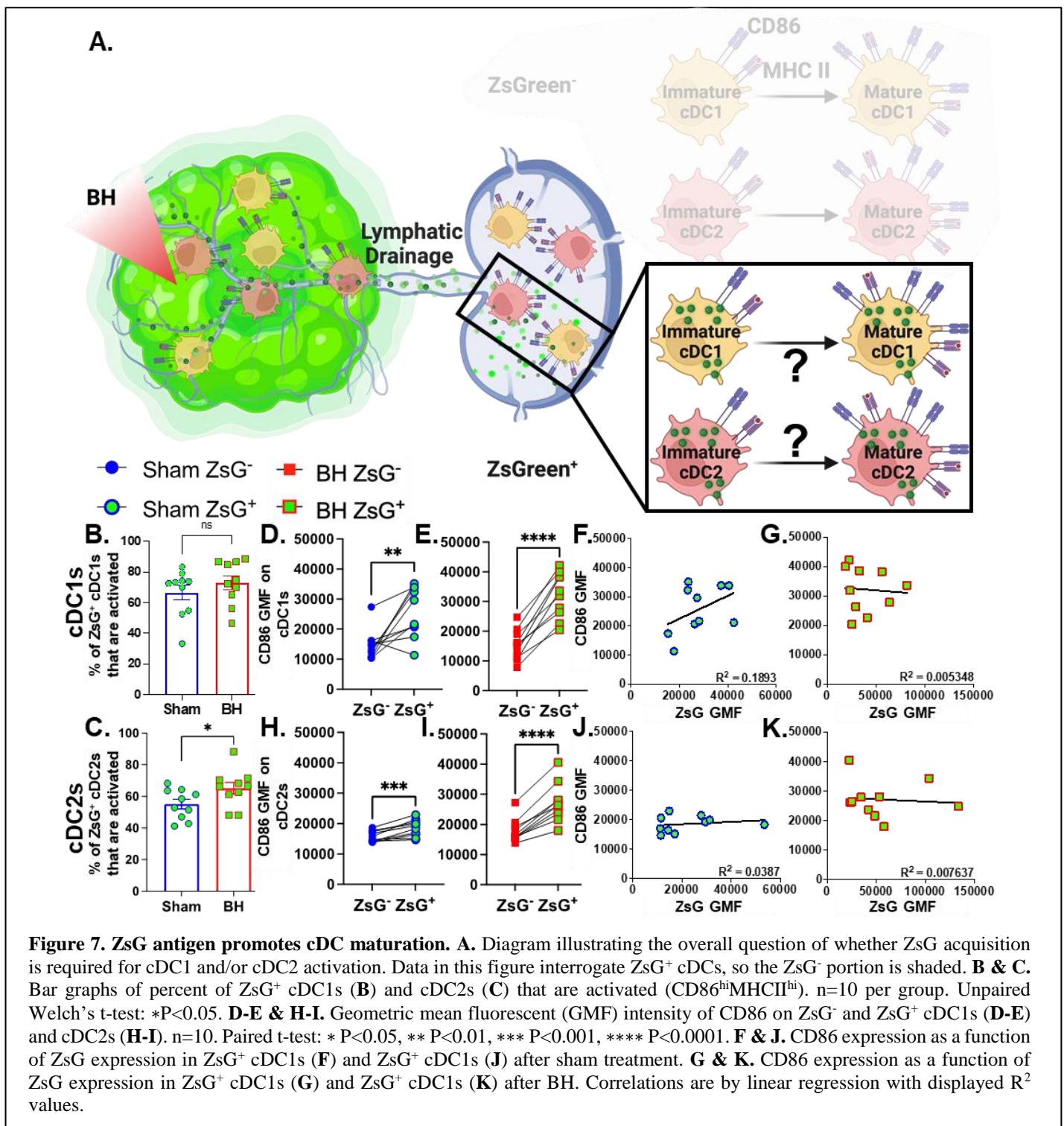


(Figure 6D and G) and percentages of activated ZsG⁻ cDCs (Figure 6E and H) between sham control and BH treated cohorts. These results indicate that BH alone is not inducing the cDC activation that we observed in Figure 5. Instead, activation only occurs as a consequence of ZsG acquisition.

Tumor Antigen Acquisition Promotes Conventional Dendritic Cell Activation

We next interrogated ZsG⁺ cDC1s and cDC2s to understand the extent to which antigen acquisition was responsible for stimulating cDC activation (Figure 7A). While the majority of ZsG⁺ cDC1s and cDC2s are activated at baseline (Figure 7B and 7C), BH did significantly increase the percentage of ZsG⁺ cDC2s that are activated (Figure 7C). Next, we compared ZsG⁻ and ZsG⁺ cDC subsets to ascertain whether ZsG alone is capable of eliciting cDC activation. Importantly, we compared these populations in the same TDLN to account for any potential differences in response to BH. The baseline presence of ZsG, in the absence of BH, correlates with higher CD86 expression on cDC1s (Figure 7D) and cDC2s (Figure 7H). However, BH further increased CD86 levels on



ZsG⁺ cDC1s (Figure 7E) and ZsG⁺ cDC2s (Figure 7I). This suggests there is a qualitative difference in cDC activation after tumor antigen acquisition as a consequence of BH.

To better understand the quality of BH-induced cDC activation, we compared BH-induced CD86 expression levels in cDCs to those elicited by administration of a TLR3 agonist (i.e., polyinosinic-polycytidylic acid with poly-L-lysine double-stranded RNA [polyI:CLC]) that is known to be a highly potent driver of cDC activation (Figure S8). In this experiment, ZsG⁺ cDCs in TDLNs of saline-treated control mice also exhibited elevated CD86 expression when compared to ZsG⁻ cDCs (Figure S8A and S8C). From there, as expected, PolyI:CLC massively increased

CD86 expression on the surface of cDCs. Furthermore, the trend that ZsG⁺ cDCs express higher levels of CD86 in response to BH was maintained with polyI:CLC treatment (Figure S8B and S8D). Thus, while BH elicits cDC activation in an antigen-dependent manner, the magnitude of the activation response does not match that generated with direct TLR3 agonism.

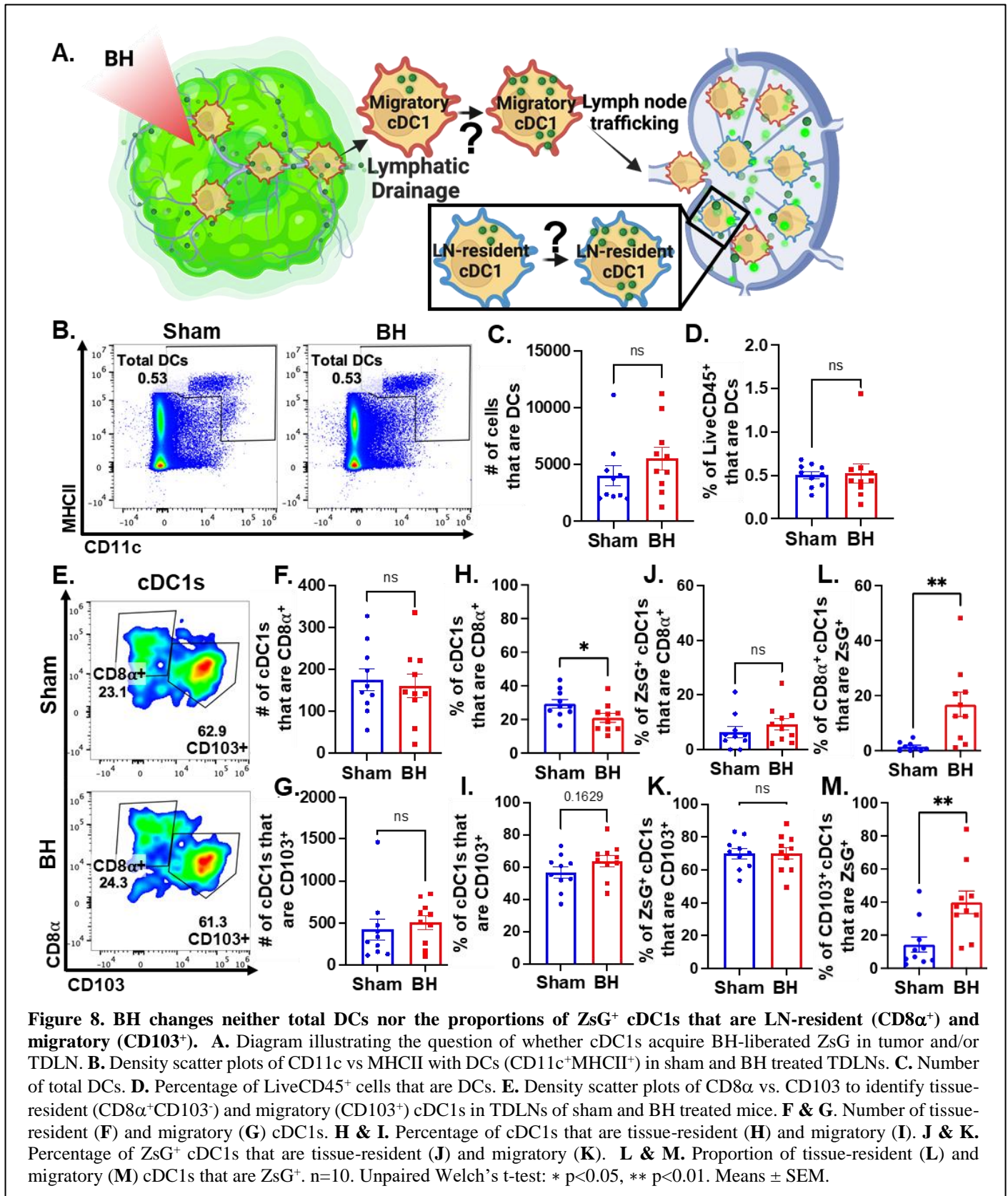
We then examined whether the increased activation that accompanies ZsG presence in cDCs after BH is reflective of the amount of ZsG acquisition or whether there is a qualitative difference in ZsG with respect to cDC activation. We hypothesized that if increases in the activation of ZsG⁺ cDCs observed after BH were simply a function of acquiring more antigen, a greater amount of acquired ZsG (i.e., ZsG GMF) would lead to greater expression levels of CD86. Nonetheless, we found no correlation between the amount of ZsG in either cDC1 or cDC2 and the level of CD86 expression for either sham (Figure 7F and J) or BH (Figure 7G and K) treated mice. Therefore, while the presence of ZsG tumor antigen presence correlates with CD86 expression on the surface of cDCs, the lack of correlation between the amount of ZsG acquired and the surface level expression of activation marker CD86 suggests that additional stimuli, such as a DAMP(s), are complexed with ZsG after BH and are required for the elevated CD86 expression.

Boiling Histotripsy Does Not Alter Total DCs or Migratory Proportions of cDC1s

There is evidence that BH can augment DC migration to the TDLN (10), but it is not known whether DCs, specifically cDCs, acquire antigen intratumorally or in the TDLN (Figure 8A). To address this question, we examined total DCs in the TDLN (Figure 8B) and observed no change in DC representation (Figure 8C and 8D). We also examined the representation of tissue-resident (CD8 α ⁺) and migratory (CD103⁺) cDC1s (Figure 8E) in TDLN, observing no changes in the numbers of CD8 α ⁺ and CD103⁺ cDC1s (Figure 8F and 8G), percentages of ZsG⁺ cDC1s that are CD8 α ⁺ and CD103⁺ (Figure 8J and 8K), and percentage of cDC1s that are CD103⁺ (Figure 8I). Though the percentage of tissue-resident cDC1s was significantly decreased (Figure 8H), we do not think this is biologically significant as the migratory cDC1s did not change (Figure 8I). Additionally, the proportions of tissue-resident (Figure 8L) and migratory (Figure 8M) cDC1s that are ZsG⁺ significantly increased (i.e., there was no differential increase between tissue-resident and migratory cDC1s). These results suggest that the increase in ZsG-tumor antigen observed for cDC1s is due to the acquisition of cell-free tumor antigen that flows to the TDLN after being liberated by BH.

Discussion

The intent of this study was to fill crucial gaps in our understanding of how BH affects key elements of the cancer immunity cycle, in particular the relationship between tumor ablation and tumor antigen acquisition by cDCs, and the allied activation of cDCs, both of which are critical to the subsequent activation of tumor-specific T cells. By deploying a sparse scan BH treatment regimen that yields abscopal control of B16F10 melanoma tumors expressing a ZsG model antigen, we were able to make the first ever direct measurements of (i) the dynamics of tumor antigen trafficking to TDLNs after BH, (ii) the identity of immune cell types that acquire BH-liberated antigen, including antigen partitioning amongst cDCs, (iii) how cDC maturation is affected by BH and the role of antigen acquisition in this process, and (iv) whether tumor antigen is dominantly acquired by cDCs in the tumor or TDLN. We observed a striking increase in tumor antigen presence in CD45⁺ immune cells in the TDLN 24h after BH, which abates by 96h post-ablation. Within TDLNs, B cells, macrophages, monocytes, and granulocytes, as well as both cDC1s and cDC2s, all acquired markedly more tumor antigen after BH. Notably, BH drove significant activation of both cDC subsets, with a more detailed analysis of our flow cytometry data revealing that (i) cDC activation was dependent upon tumor antigen acquisition and (ii) the tumor antigen liberated by BH is likely complexed with a DAMP. Because the increase in tumor antigen-bearing cDCs in TDLN



338 after BH did not correlate with an increase in total DC presence in the TDLN or a marker of cDC
 339 migration (CD103), we posit that cDCs do not traffic to the TDLN with antigen, but rather acquire
 340 antigen as it flows through afferent lymph vessels into the TDLN. In all, our results illuminate
 341 numerous previously unknown features of how BH, applied with a monotherapy protocol that elicits
 342 abscopal tumor control, drives tumor antigen trafficking to TDLN and instructs DC function. Going

343 forward, such information will be invaluable for (i) rationally tuning BH treatments for optimal
344 immunological tumor control and (ii) selecting immunotherapies, as well as their administration
345 timings, for improved combination treatments.

346 *Dynamics of Tumor Antigen Trafficking to the TDLN*

347 We determined that BH drives a nearly 3-fold increase in the proportion of antigen positive
348 immune cells at 24 h, with a return to baseline by 96 h after BH treatment. We chose 24 h as the
349 timepoint in all subsequent studies based on this finding. We also emphasize that this time point is
350 commonly used in other studies of antigen and DC trafficking (27–30) and is appropriate for this
351 particular application. Indeed, the choice of the 24h timepoint permits identification of both small
352 soluble antigens, such as ZsG (26 kDa m.w.) that reach the TDLN in an acellular fashion within
353 minutes (27–29, 31, 32), as well as DCs that acquire antigen in the tumor microenvironment and
354 may take ~18 hours to traffic to the TDLN (33). Notably, molecules exceeding ~60-70 kDa appear
355 to need a cell (e.g., migratory CD103⁺ cDC1s) to traffic the antigen from peripheral tissues (e.g.,
356 tumor) to the TDLN (28, 29), thus our use of the relatively small ZsG antigen permits assessment
357 of antigen trafficking via both means.

358 We also provide considerable evidence that tumor antigen acquisition after BH is
359 independent of cDC trafficking from the BH-treated tumor to the TDLN. First, enhanced tumor
360 antigen presence was observed after BH in cell types that do not migrate from the tumor to TDLN
361 (e.g., B cells). Second, within the cDC1 and cDC2 subsets, we observed no changes in total cDCs,
362 nor in cDCs containing ZsG. This result suggests that cDCs are acquiring tumor antigen in the
363 TDLN. Third, when we quantified CD8 α ⁺ (tissue-resident) and CD103⁺ (migratory) cDC1s, we
364 found neither an increase in the CD103⁺ migratory population in TDLN in response to BH, nor an
365 increase in the presence of ZsG tumor antigen in these cells. Together, these data strongly argue
366 that BH treatment does not promote the migration of cDC to TDLN. Rather, cell-free tumor debris
367 is reaching the TDLN. That said, these results do run counter to another study wherein BH increased
368 the numbers of total and transferred (i.e., injected intratumoral CSFE-labelled bone-marrow derived
369 DCs [BMDCs] two days post BH treatment) DCs in the TDLN in the context of MC-38 colorectal
370 cancer (10). The most obvious difference between our studies is the difference in tumor model (i.e.,
371 3-4x10⁵ B16F10-ZsG vs 1x10⁶ MC-38 (10)). At baseline, MC-38 grows slower and has higher T
372 cell, NK cell and cDC infiltration. Moreover, MC-38 tumors have a superior response to anti-PD-
373 1 therapy (34). A more nuanced difference appears in the number of BH application points per
374 tumor. While our treatments entailed 20 to 79 sonications per tumor, Hu et al. applied 12 to 16
375 sonications (10). Our BH ablation regimen appears to be more aggressive given similarities in focal
376 size and transducer frequency. These results may indicate that DC-sparing ablation regimens can
377 be crafted to better promote DC trafficking to the TDLN, though the therapeutic necessity of such
378 DCs has yet to be determined. An alternate hypothesis is that intratumoral DCs do not play a
379 significant role in the immunological response to BH in melanoma. In that case, sparing DCs from
380 BH ablation will confer no benefit. Thus, increasing the intensity and/or fraction of BH ablation to
381 liberate more tumor antigen may further augment favorable responses. Another caveat to this
382 interpretation is that we only examined cDCs 24h after BH. It is possible that a small number of
383 migratory cDCs emerge later, although we determined that no increase in tumor antigen in TDLN
384 is evident at 96 post BH. These results have important implications for choosing tumor models, BH
385 ablation fractions, and timepoints in future studies aimed at combining BH with immunotherapies.

386 *Partitioning of Tumor Antigen in cDCs in TDLN*

387 Another important objective of our studies was to determine whether BH-liberated tumor
388 antigen is preferentially acquired by either cDC1s or cDC2s in the TDLN, as this may influence the
389 subsets of T cells primarily stimulated by BH. We found an increase in the number and proportion
390 of antigen positive cells in both cDCs. Because cDC1s primarily activate CD8⁺ T cells (21–23),

391 while cDC2s are required for initial priming of CD4 T cells (21), these results indicate that we
392 should not expect a biasing toward CD4⁺ or CD8⁺ T cell activation due to uneven cDC tumor
393 antigen acquisition. Interestingly, the cDC2 subset did exhibit more antigen per cell, which may
394 suggest that cDC2s express phagocytosis receptors that are more adept at acquiring BH-liberated
395 antigen and/or that cDC2s are preferentially positioned in the TDLN (i.e., close to the lymphatic
396 cannulae) to acquire this antigen.

397 *Activation of cDC in TDLN as a Function of BH and Tumor Antigen Acquisition*

398 Our studies have revealed unexpected relationships between BH-mediated tumor antigen
399 liberation and the activation state of cDCs in the TDLN. Indeed, we found that only ZsG⁺ cDCs
400 exhibit increased CD86 expression as a function of BH treatment. Given that previous studies have
401 documented the release of DAMPs capable of driving CD86 expression on BMDC in vitro (8), as
402 well as antigen-agnostic activation of DCs after BH in mouse lymphoma (19), we had expected a
403 similar global activation of cDCs independent from the acquisition of tumor antigen. The current
404 data suggests that either the process of acquiring tumor antigen drives cDC activation or that
405 stimulatory molecules complexed with the tumor antigens are responsible for cDC activation.
406 Moreover, we determined that the level of CD86 expression was higher on ZsG⁺ cDC from BH
407 treated TDLN compared to sham controls, yet we did not observe a proportional increase in CD86
408 expression as cDC acquired more tumor antigen after BH. The tentative conclusion from these
409 observations is that the increased level of cDC activation seen after BH is not simply a function of
410 there being more tumor antigen available to engulf. Instead, exposure to BH may modify the tumor
411 antigen in a manner that promotes cDC activation, perhaps by complexing it with a DAMP.

412 **Materials and Methods**

413 **Cell line and animal maintenance**

414 The B16F10-ZsGreen cell line was a kind gift from Dr. Matthew Krummel at the University
415 of California, San Francisco (35). Cells were maintained in RPMI-1640+L-Glutamine (Gibco
416 #11875-093) supplemented with 10% Fetal Bovine Serum (FBS, Gibco #16000-044) at 37°C and
417 5% CO₂ (Thermo Fisher Scientific, Heracell 150i Cat#51-032-871). Thawed cells were cultured
418 for up to three passages and maintained in logarithmic growth phase for all experiments. Cells
419 tested negative for mycoplasma prior to freezing.

420 All mouse experiments were conducted in accordance with the guidelines and regulations
421 of the University of Virginia and approved by the University of Virginia Animal Care and Use
422 Committee. Eight-week-old to ten-week-old male C57Bl/6J mice were obtained from The Jackson
423 Laboratory (Jax #000664). 3-4x10⁵ B16F10-ZsGreen cells were implanted subcutaneously (s.c.)
424 into the right flank of mice after shaving through a 25G x 1 ½ in needle (BD PrecisionGlide Needle
425 #305127). For the growth control and survival study, 4x10⁵ B16F10-ZsGreen cells were s.c.
426 implanted into the right and left flanks of mice and treated with sham/BH 14 days post-inoculation.
427 Mice were housed on a 12- hour/12- hour light/dark cycle and supplied food ad libitum. Tumor
428 outgrowth was monitored via digital caliper measurements. Tumor volume was calculated as
429 follows: volume = (length×width²)/2. Thirteen- or fourteen-days following tumor implantation,
430 mice were randomized into groups in a manner that ensured matching of mean starting tumor
431 volume across experimental groups.

432 **In vivo ultrasound-guided boiling histotripsy**

433 Mice underwent sham or BH treatment 13- or 14-days post-inoculation. On treatment day,
434 mice were anesthetized with an intraperitoneal (i.p.) injection of ketamine (50 mg/kg; Zoetis) and
435 dexdomitor (0.25 mg/ kg; Pfizer) in sterilized 0.9% saline (Hospira #PAA128035). Dexdomitor
436

438 was reversed with a s.c. injection of atipamezole hydrochloride (0.25 mL in 10 mL saline, 0.4 mL
439 s.c., Antisedan, Zoetis) after sham or BH treatment. Right flanks of mice were shaved, after which
440 BH was performed using an in-house built ultrasound-guided FUS system. This includes
441 incorporation of ultrasound visualization/guidance orthogonal to the focal axis of the therapy
442 transducer. The system uses one of two linear imaging arrays: 1) Acuson Sequoia 512, 15L8
443 imaging probe, 8 MHz, 25 mm field (Siemens, Inc.) width or 2) Acuson S2000 Helix Evolution
444 Touch, 14L5 SP imaging probe, 10 MHz, 25 mm field width (Siemens, Inc.). A 1.1 MHz center-
445 frequency, single-element therapy transducer H-101 (Sonic Concepts Inc., Bothel, WA) was used
446 in combination with an arbitrary function generator (Tektronix, AFG 3052C) and amplifier (E&I,
447 1040L) to produce BH treatments. This therapy transducer had an active diameter of 64 mm and
448 radius of curvature of 63.2 mm (i.e., the geometric focal distance). The transducer was operated at
449 third harmonic (3.28 MHz), with a -6dB focal size of 0.46 mm x 0.46 mm x 3.52 mm = ~0.39 mm³.
450 Both the imaging and treatment transducers were ultrasonically coupled to the animal using
451 degassed, deionized water at 37°C during the duration of each BH treatment. BH was applied in a
452 pulsed fashion for 10 s, at a peak negative pressure = 21 MPa, pulse repetition frequency = 4 Hz,
453 pulse length = 3 ms, with treatment points spaced 1 mm in a rectangular grid pattern and 2 planes
454 of treatment, which were separated by 2 mm. The treatment scheme is outlined in Figure S1. Sham
455 treatment comprised of fully submerging the flank tumor in the 37°C water bath for 6 minutes.

456

457 **PolyI:CLC delivery**

458 PolyI:CLC (Oncovir, Inc., Hiltonol®) was injected i.p. at 13 days post-inoculation with 75
459 µg/0.1 mL diluted with sterilized 0.9% saline. Flow cytometry was performed 24 hr after injection.

460

461 **Flow Cytometry**

462 At 13 days post-tumor inoculation, tumor draining lymph nodes (TDLNs) - axial and
463 brachial on the right side – as well as contralateral non-tumor draining lymph nodes were excised
464 and pooled. LNs were subjected to manual homogenization (Wheaton, Tenbroeck Tissue Grinder
465 #62400-518) and filtered through 100 µm filter mesh (Genesee Scientific # 57-103) to generate
466 single-cell suspensions, which were then washed in 1X PBS, centrifuged at 1200 RPM for 5 minutes
467 (Eppendorf 5180) and stained for cell viability using Fixable Live/Dead Blue for 30 min at 4°C.
468 Next, the samples were exposed to anti-mouse CD16/32 to block Fc gamma receptors for 15 min
469 at 4°C. Afterwards, cells were washed with FACS buffer, centrifuged, and resuspended in a mixture
470 of Brilliant Stain Buffer and FACS+2% normal mouse serum (Valley Biomedical, Inc., #AS3054)
471 at a ratio of 1:9, respectively, and stained for 30 min at 4°C with fluorescent monoclonal antibodies
472 for CD45, CD11b, Ly-6G, Ly-6C, F4/80, CD11c, MHCII, XCR1, SIRPα, CD19, CD3, CD8α,
473 CD86, CCR7 and CD103. Antibody clone information, supplier name and catalog number can be
474 found in Table S2. Lastly, cells were fixed in 1X BD FACS Lysis for 10 min at room temperature,
475 and then resuspended in FACS buffer for running. Flow cytometry was performed with the Cytex
476 Aurora Borealis (Cytex Biosciences) and SpectroFlo v3.0.3 software (Cytex Biosciences). Data
477 was analyzed using FlowJo 10 software (FlowJo, LLC). All gating strategies can be found in
478 Figures S2, S4, S6 and S8.

479

480 **Statistical Analyses**

481 Most statistical analyses were performed in GraphPad Prism 9 (GraphPad Software). Mouse
482 survival was analyzed using a Kaplan-Meier analysis and a log-rank (Mantel-Cox) test was used to
483 assess significance. When comparing two groups of flow cytometry data or area under the curve

484 (AUC; i.e., sham vs BH), an unpaired, two-tailed t-test with Welch’s correction (i.e., did not assume
485 equal standard deviations) was performed. A paired t-test was used to compare within group
486 differences based on ZsG positivity (i.e., sham ZsG⁻ vs sham ZsG⁺; BH ZsG⁻ vs BH ZsG⁺). Groups
487 of flow cytometry summary data across time were compared using a full-model, two-way analysis
488 of variance (ANOVA) and Tukey post-hoc tests to assess significance of factors (i.e., time [factor
489 1] and sham/BH [factor 2]) and between individual groups, respectively. All figures show the mean
490 ± standard error of the mean (SEM). P-values and significance are specified in figure legends. All
491 figure schematics were made with BioRender.com.

492 Tumor growth data was modeled in MATLAB 2022b using non-linear least squares with a
493 logistics model (36–38) out to day 35 post-inoculation to account for mouse drop out (i.e., tumor
494 size met one of the humane endpoint criteria) for each individual mouse. The resulting curves were
495 averaged together. The modeled data was appended to actual tumor data up until day 35 (e.g., if the
496 mouse dropped out at day 25, only days 26 through 35 of the modeled data are used). The following
497 variation of a logistic model was used (Eq. 1).

$$V(t) = \frac{V_{max}}{1 + r \cdot e^{(-a \cdot t)}} - \frac{V_{max}}{1 + r}, V(0) = 0 \quad (\text{Eq. 1})$$

499 The fitted parameters are “r” and “a” while, if the maximum tumor volume of the raw data
500 is less than 4000 mm³, V_{max} is 4000 mm³, otherwise, V_{max} is set to the maximum tumor volume. The
501 value of 4000 mm³ was chosen because this is roughly the largest volume a tumor can achieve
502 given the humane endpoint criteria. The R², “r” and “a” values can be found in Table S1.
503 Comparisons of these logistic average tumor curves between treatment groups were performed with
504 a full model, two-way repeated-measures ANOVA with two factors (i.e., time [repeated-measures]
505 and sham/BH) and corresponding interaction terms using the Geisser-Greenhouse correction. The
506 fixed effect of BH treatment was used to determine significance. Furthermore, to summarize the
507 logistic average tumor growth curves with a single parameter, we calculated the AUC from day 14
508 to 35 for the averaged curves using the trapezoid rule (39).

509
510

511 References

- 512 1. American Cancer Society - ACS, Melanoma Survival Rates | Melanoma Survival Statistics
513 (2021).
- 514 2. P. Bonaventura, T. Shekarian, V. Alcazer, J. Valladeau-Guilemond, S. Valsesia-Wittmann,
515 S. Amigorena, C. Caux, S. Depil, Cold Tumors: A Therapeutic Challenge for
516 Immunotherapy. *Front. Immunol.* **10** (2019), doi:10.3389/fimmu.2019.00168.
- 517 3. S. Han, W. H. Shuen, W.-W. Wang, E. Nazim, H. C. Toh, Tailoring precision
518 immunotherapy: coming to a clinic soon? *ESMO Open.* **5**, e000631 (2020).
- 519 4. A. Kheirloom, M. T. Silvestrini, E. S. Ingham, L. M. Mahakian, S. M. Tam, S. K.
520 Tumbale, J. Foiret, N. E. Hubbard, A. D. Borowsky, K. W. Ferrara, Combining activatable
521 nanodelivery with immunotherapy in a murine breast cancer model. *J. Control. Release.*
522 **303**, 42–54 (2019).
- 523 5. N. D. Sheybani, R. J. Price, Perspectives on recent progress in focused ultrasound
524 immunotherapy. *Theranostics.* **9**, 7749–7758 (2019).
- 525 6. Z. Xu, T. L. Hall, E. Vlaisavljevich, F. T. Lee, Histotripsy: the first noninvasive, non-
526 ionizing, non-thermal ablation technique based on ultrasound. *Int. J. Hyperthermia.* **38**, 561
527 (2021).
- 528 7. A. Hendricks-Wenger, R. Hutchison, E. Vlaisavljevich, I. C. Allen, Immunological Effects
529 of Histotripsy for Cancer Therapy. *Front. Oncol.* **11** (2021), ,
530 doi:10.3389/fonc.2021.681629.

- 531 8. Z. Hu, X. Y. Yang, Y. Liu, M. A. Morse, H. K. Lysterly, T. M. Clay, P. Zhong, Y. Y. Xiao,
532 Y. Liu, M. A. Morse, H. K. Lysterly, T. M. Clay, P. Zhong, Release of endogenous danger
533 signals from HIFU-treated tumor cells and their stimulatory effects on APCs. *Biochem.*
534 *Biophys. Res. Commun.* **335**, 124–131 (2005).
- 535 9. G. R. Schade, Y. N. Wang, S. D'Andrea, J. H. Hwang, W. C. Liles, T. D. Khokhlova,
536 Boiling Histotripsy Ablation of Renal Cell Carcinoma in the Eker Rat Promotes a Systemic
537 Inflammatory Response. *Ultrasound Med. Biol.* **45**, 137–147 (2019).
- 538 10. Z. Hu, X. Y. Yang, Y. Liu, G. Sankin, E. Pua, M. A. Morse, H. K. K. Lysterly, T. M. Clay,
539 P. Zhong, G. Sankin, E. Pua, M. A. Morse, H. K. K. Lysterly, T. M. Clay, P. Zhong,
540 Investigation of HIFU-induced anti-tumor immunity in a murine tumor model. *AIP Conf.*
541 *Proc.* **829**, 241–245 (2006).
- 542 11. Y. N. Wang, T. D. Khokhlova, S. Buravkov, V. Chernikov, W. Kreider, A. Partanen, N.
543 Farr, A. Maxwell, G. R. Schade, V. A. Khokhlova, Mechanical decellularization of tissue
544 volumes using boiling histotripsy. *Phys. Med. Biol.* **63** (2018), doi:10.1088/1361-
545 6560/aaef16.
- 546 12. Y. Xing, X. Lu, E. C. Pua, P. Zhong, The effect of high intensity focused ultrasound
547 treatment on metastases in a murine melanoma model. *Biochem. Biophys. Res. Commun.*
548 **375**, 645–650 (2008).
- 549 13. R. J. E. van den Bijgaart, D. C. Eikelenboom, M. Hoogenboom, J. J. Fütterer, M. H. den
550 Brok, G. J. Adema, Thermal and mechanical high-intensity focused ultrasound:
551 perspectives on tumor ablation, immune effects and combination strategies. *Cancer*
552 *Immunol. Immunother.* **66**, 247–258 (2017).
- 553 14. V. A. Khokhlova, J. B. Fowlkes, W. W. Roberts, G. R. Schade, Z. Xu, T. D. Khokhlova, T.
554 L. Hall, A. D. Maxwell, Y. N. Wang, C. A. Cain, Histotripsy methods in mechanical
555 disintegration of tissue: Towards clinical applications. *Int. J. Hyperth.* **31**, 145–162 (2015).
- 556 15. M. Hoogenboom, D. Eikelenboom, M. H. den Brok, A. Heerschap, J. J. Fütterer, G. J.
557 Adema, Mechanical High-Intensity Focused Ultrasound Destruction of Soft Tissue:
558 Working Mechanisms and Physiologic Effects. *Ultrasound Med. Biol.* **41**, 1500–1517
559 (2015).
- 560 16. A. D. Maxwell, P. V. Yuldashev, W. Kreider, T. D. Khokhlova, G. R. Schade, T. L. Hall,
561 O. A. Sapozhnikov, M. R. Bailey, V. A. Khokhlova, A Prototype Therapy System for
562 Transcutaneous Application of Boiling Histotripsy. *IEEE Trans. Ultrason. Ferroelectr.*
563 *Freq. Control.* **64**, 1542–1557 (2017).
- 564 17. C. Cain, L. Crum, Disintegration of Tissue Using High Intensity Focused Ultrasound :
565 (2012).
- 566 18. K. B. Bader, E. Vlaisavljevich, A. D. Maxwell, For Whom the Bubble Grows: Physical
567 Principles of Bubble Nucleation and Dynamics in Histotripsy Ultrasound Therapy.
568 *Ultrasound Med. Biol.* **45**, 1056–1080 (2019).
- 569 19. R. J. E. van den Bijgaart, V. E. Mekers, F. Schuurmans, T. K. Raaijmakers, M. Wassink,
570 A. Veltien, E. Dumont, A. Heerschap, J. J. Fütterer, G. J. Adema, Mechanical high-
571 intensity focused ultrasound creates unique tumor debris enhancing dendritic cell-induced
572 T cell activation. *Front. Immunol.* **13**, 1–13 (2022).
- 573 20. S. Abe, H. Nagata, E. J. Crosby, Y. Inoue, K. Kaneko, C. X. Liu, X. Yang, T. Wang, C. R.
574 Acharya, P. Agarwal, J. Snyder, W. Gwin, M. A. Morse, P. Zhong, H. K. Lysterly, T. Osada,
575 Combination of ultrasound-based mechanical disruption of tumor with immune checkpoint
576 blockade modifies tumor microenvironment and augments systemic antitumor immunity. *J.*
577 *Immunother. Cancer.* **10**, e003717 (2022).
- 578 21. M. Binnewies, A. M. Mujal, J. L. Pollack, A. J. Combes, E. A. Hardison, K. C. Barry, J.
579 Tsui, M. K. Ruhland, K. Kersten, M. A. Abushawish, M. Spasic, J. P. Giurintano, V. Chan,
580 A. I. Daud, P. Ha, C. J. Ye, E. W. Roberts, M. F. Krummel, Unleashing Type-2 Dendritic

- 581 Cells to Drive Protective Antitumor CD4+ T Cell Immunity. *Cell*. **177**, 556-571.e16
582 (2019).
- 583 22. J. Y. Shin, C. Y. Wang, C. C. Lin, C. L. Chu, A recently described type 2 conventional
584 dendritic cell (cDC2) subset mediates inflammation. *Cell. Mol. Immunol.* **17**, 1215–1217
585 (2020).
- 586 23. N. Caronni, G. M. Piperno, F. Simoncello, O. Romano, S. Vodret, Y. Yanagihashi, R.
587 Dress, C. A. Dutertre, M. Bugatti, P. Bourdeley, A. Del Prete, T. Schioppa, E. M. C.
588 Mazza, L. Collavin, S. Zacchigna, R. Ostuni, P. Guermonprez, W. Vermi, F. Ginhoux, S.
589 Biccato, S. Nagata, F. Benvenuti, TIM4 expression by dendritic cells mediates uptake of
590 tumor-associated antigens and anti-tumor responses. *Nat. Commun.* **12**, 2237 (2021).
- 591 24. G. O. Oosterhof, E. B. Cornel, G. A. Smits, F. M. Debruyne, J. A. Schalken, Influence of
592 high-intensity focused ultrasound on the development of metastases. *Eur. Urol.* **32**, 91–5
593 (1997).
- 594 25. G. O. N. Oosterhof, E. B. Cornel, G. A. H. J. Smits, F. M. J. Debruyne, J. A. Schalken, The
595 influence of high-energy shock waves on the development of metastases. *Ultrasound Med.*
596 *Biol.* **22**, 339–344 (1996).
- 597 26. Q. Yu, Y. Yao, X. Zhu, Y. Gao, Y. Chen, R. Wang, P. Xu, X. Wei, L. Jiang, In Vivo Flow
598 Cytometric Evaluation of Circulating Metastatic Pancreatic Tumor Cells after High-
599 Intensity Focused Ultrasound Therapy. *Cytom. Part A.* **97**, 900–908 (2020).
- 600 27. C. P. Loo, N. A. Nelson, R. S. Lane, J. L. Booth, S. C. Loprinzi Hardin, A. Thomas, M. K.
601 Slifka, J. C. Nolz, A. W. Lund, Lymphatic Vessels Balance Viral Dissemination and
602 Immune Activation following Cutaneous Viral Infection. *Cell Rep.* **20**, 3176–3187 (2017).
- 603 28. M. Sixt, N. Kanazawa, M. Selg, T. Samson, G. Roos, D. P. Reinhardt, R. Pabst, M. B.
604 Lutz, L. Sorokin, The conduit system transports soluble antigens from the afferent lymph
605 to resident dendritic cells in the T cell area of the lymph node. *Immunity.* **22**, 19–29 (2005).
- 606 29. V. Manolova, A. Flace, M. Bauer, K. Schwarz, P. Saudan, M. F. Bachmann, Nanoparticles
607 target distinct dendritic cell populations according to their size. *Eur. J. Immunol.* **38**, 1404–
608 1413 (2008).
- 609 30. K. A. Pape, D. M. Catron, A. A. Itano, M. K. Jenkins, The Humoral Immune Response Is
610 Initiated in Lymph Nodes by B Cells that Acquire Soluble Antigen Directly in the
611 Follicles. *Immunity.* **26**, 491–502 (2007).
- 612 31. S. F. Gonzalez, S. E. Degn, L. A. Pitcher, M. Woodruff, B. A. Heesters, M. C. Carroll,
613 Trafficking of B cell antigen in lymph nodes. *Annu. Rev. Immunol.* **29**, 215–233 (2011).
- 614 32. D. M. Catron, A. A. Itano, K. A. Pape, D. L. Mueller, M. K. Jenkins, Visualizing the first
615 50 hr of the primary immune response to a soluble antigen. *Immunity.* **21**, 341–347 (2004).
- 616 33. A. A. Itano, M. K. Jenkins, Antigen presentation to naive CD4 T cells in the lymph node.
617 *Nat. Immunol.* **4**, 733–739 (2003).
- 618 34. S. T. T. Schetters, E. Rodriguez, L. J. W. Kruijssen, M. H. W. Crommentuijn, L. Boon, J.
619 Van Den Bossche, J. M. M. Den Haan, Y. Van Kooyk, Monocyte-derived APCs are central
620 to the response of PD1 checkpoint blockade and provide a therapeutic target for
621 combination therapy. *J. Immunother. Cancer.* **8**, 1–16 (2020).
- 622 35. M. B. Headley, A. Bins, A. Nip, E. W. Roberts, M. R. Looney, A. Gerard, M. F. Krummel,
623 Visualization of immediate immune responses to pioneer metastatic cells in the lung.
624 *Nature.* **531**, 513–7 (2016).
- 625 36. B. Ribba, G. Kaloshi, M. Peyre, D. Ricard, V. Calvez, M. Tod, B. Čajavec-Bernard, A.
626 Idbaih, D. Psimaras, L. Dainese, J. Pallud, S. Cartalat-Carel, J. Y. Delattre, J. Honorat, E.
627 Grenier, F. Ducray, A tumor growth inhibition model for low-grade glioma treated with
628 chemotherapy or radiotherapy. *Clin. Cancer Res.* **18**, 5071–5080 (2012).
- 629 37. A. Yin, D. J. A. R. Moes, J. G. C. van Hasselt, J. J. Swen, H. J. Guchelaar, A Review of
630 Mathematical Models for Tumor Dynamics and Treatment Resistance Evolution of Solid

- 631 Tumors. *CPT Pharmacometrics Syst. Pharmacol.* **8**, 720–737 (2019).
632 38. P. Gerlee, The model muddle: In search of tumor growth laws. *Cancer Res.* **73**, 2407–2411
633 (2013).
634 39. L. W. Patten, P. Blatchford, M. Strand, A. M. Kaizer, Assessing the performance of
635 different outcomes for tumor growth studies with animal models. *Anim. Model. Exp. Med.*
636 **5**, 248–257 (2022).

637
638

639 **Acknowledgments**

640 We thank the Flow Cytometry Core Facility of the University of Virginia for the use of
641 their cytometers. This core is supported by the National Cancer Institute P30-CA044579 Center
642 Grant. We would like to thank Dr. Matthew Krummel for his gift of the B16F10-ZsGreen cell
643 line.

644

645 **Funding**

646 Supported by National Institutes of Health grant R01EB030007 to RJP and TNJB.

647

648 **Author contributions**

649 EAT and LEP contributed equally to all areas.

650 Conceptualization: EAT, LEP, TNJB, RJP

651 Methodology: EAT, LEP, FRE, ASM, MRE, TNJB, RJP

652 Formal analysis and investigation: EAT, LEP, FRE, ASM

653 Writing - original draft preparation: EAT, LEP

654 Writing - review and editing: EAT, LEP, FRE, ASM, MRE, TNJB, RJP

655 Funding acquisition: TNJB, RJP

656 Resources: MRE, TNJB, RJP

657 Supervision: MRE, TNJB, RJP

658

659 **Competing interests**

660 The authors declare that they have no competing interests.

661

662 **Data and materials availability**

663 All data are available in the main text or supplementary materials and are available upon request.

664